ASI Version 5 Sea Ice Concentration User Guide

Institute of Environmental Physics, University of Bremen

Christian Melsheimer

Version V0.9.4 (August 9, 2024)

Change record

- 2020-07-23: Updated EASE grid information URL.
- 2034-08-09: Added paragraph about land contamination

Contents

1 Introduction

This Document is intended for users of the ASI sea ice concentration product from the University of Bremen, Institute of Environmental Physics (IUP), available at https:seaice.uni-bremen.de.

These sea ice concentration data are retrieved with the ARTIST Sea Ice (ASI) algorithm (Spreen et al., 2008) which is applied to microwave radiometer data of the sensors AMSR-E (Advanced Microwave Scanning Radiometer for EOS) on the NASA satellite Aqua, and AMSR2 (Advanced Microwave Scanning Radiometer 2) on the JAXA satellite GCOM-W1.

The ASI algorithm using AMSR-E data was first implemented at IUP in 2002 and has been continuously producing sea ice concentration data since then. As several details of the processing chain have changed over the years, in 2018, all ASI ice concentration data for the Arctic and Antarctic based on AMSR-E and AMSR2 were reprocessed with exactly the same parameters, settings and software. The result are ASI data, version 5.4. The details are explained in the following sections.

2 Input Data

Details about the input data from the two sensors AMSR-E and AMSR2 are specified in Table 1

Sensor	Data	Lvl	Version	Time Range	Source
AMSR-E	raw obs. counts	1A	3	2002-06-01 - 2011-10-04	NASA/JAXA[a]
AMSR2	brightness temp.	1B	2.220.220	2 Jul 2012 – today	JAXA[b]

[a] JAXA (2003)
[b] JAXA G-Portal, https://gportal.jaxa.jp

Table 1: *Input data for the ASI algorithm. Note: Lvl = Processing Level, obs. = observation, temp. = temperature.*

Both sensors measure the brightness temperature (i.e., microwave radiance) at several frequency channels at both horizontal (H) and vertical (V) polarisation. The frequency channels relevant here are 18, 23, 37 and 89 GHz.

The input data come as two files per orbit (i.e., two half-orbits) and contain the measured values in all channels for each satellite footprint and the geographical location of each footprint – this is called swath data. The half-orbits are either descending or ascending. There are about 29 to 30 half-orbit swath files per day. The instrument is conically scanning at constant looking angle, therefore, the scan lines are circle segments. For the lower frequency channels up to 37 GHz, the spacing between successive footprints in one scan line is 10 km, and the spacing between successive scan lines is 10 km in flight direction. The 89 GHz channels have the smallest footprint size (6×4 km^2) and therefore, the spacing between footprints in a scan line is 5 km, and there is an additional feedhorn for 89 GHz that produces an additional scan line in the middle between the other scan lines. This is called the B scan. Thus, the spacing between scan lines at the 89 GHz channels is only 5 km, with alternating A and B scans. Note: The A-scan feedhorn of AMSR-E was broken after 4 November, 2004, so its data are replaced by interpolating between neighboring B-scan footprints.

3 Processing Chain

The main steps of the ASI processing chain are the following (details are described in section 3.1 to section 3.5):

- Reading swath data, AMSR-E L1A or AMSR2 L1B data; the Level 1A data are first converted to brightness temperatures using the calibration parameters which come with the L1A data; AMSR2 brightness temperatures are then converted to equivalent AMSR-E brightness temperatures
- Applying the ASI algorithm to the swath data of brightness temperatures, resulting in swath-wise sea ice concentration
- Resampling (gridding) all swath data of ice concentration of one calendar day (UTC) into polar stereographic grids
- Saving the gridded data as maps in image format and as quantitative data in HDF4, NetCDF and geoTIFF format.

3.1 AMSR-E and AMSR2 swath data

3.1.1 AMSR-E

AMSR-E Level 1A data, version 3, are used (see section 2 above). They contain raw observation counts and calibration parameters that are read and converted to brightness temperatures according to the documentation of the data [REFERENCE]. In addition, the data contain the geolocation information for each footprint. The geolocation information is then corrected following the approach by Wiebe et al. (2008)

3.1.2 AMSR2

AMSR2 Level 1B, version 2.220.220 are used (see section 2 above). They contain the calibrated brightness temperatures and the geolocation information. The ASI algorithm has been developed and validated with AMSR-E brightness temperatures. The successor instrument AMSR2 has similar, but not identical channels and channel characteristics. A regression analysis of co-located AMSR-E and AMSR2 data[1] yields coefficients for converting AMSR2 brightness temperatures into equivalent AMSR-E brightness temperatures, so the original ASI algorithm for AMSR-E can be applied. The set of coefficients used here is given in the Appendix, section B.

3.2 ASI algorithm

The ASI algorithm (Spreen et al., 2005, 2008) mainly uses the difference between the brightness temperatures at 89 GHz, V and H polarisation. The 89 GHz channels have the highest resolution of all channels of the AMSR-E and AMSR2 instrument, but more influence by the atmosphere (in particular: water vapour and cloud liquid water). This is dealt with in a bulk correction for atmospheric opacity (mainly water vapour) and by so-called weather filters.

[1] Although the scanning mechanism of the AMSR-E antenna reflector broke down in October 2011, the antenna still measured brightness temperatures well into the lifetime of AMSR2

Parameter	Meaning	Value	Note
P_0	P at 0% ice concentration	47.0 K	Arctic & Antarctic
P_1	P at 100% ice concentration	11.7 K	Arctic & Antarctic
$F_{37V,18V}$	threshold $GR_{37V,18V}$	0.045	$GR_{37V,18V} > WF_{17V,18V} : IC = 0$
$F_{23V,18V}$	threshold $GR_{23V,18V}$	0.04	$GR_{23V,18V} > WF_{23V,18V} : IC = 0$
$\min(boot)$	threshold bootstr. corr.	5%	$IC_{boot} \leq 5\% : IC = 0$

Table 2: *Parameter setting for ASI version 5.2, 5.3 and 5.4. IC is ASI ice concentration, IC_{boot} is Bootstrap ice concentration*

The polarisation difference P, defined as the difference between the 89 GHz brightness temperatures at V and H polarisation:

$$P = T_{B,89V} - T_{B,89H} \tag{1}$$

is converted into sea ice concentration using so-called tie points, i.e., fixed values of P for 0% (P_0) and 100% ice concentration (P_1). To correct for weather influences, the gradient ratios of channel pairs, defined as, e.g.,

$$GR_{37V,18V} = \frac{T_{B,37V} - T_{B,18V}}{T_{B,37V} + T_{B,18V}} \tag{2}$$

are checked, and the ice concentration is set to 0% where $GR_{37V,18V}$ or $GR_{23V,18V}$ are above respective thresholds. Finally the ice concentration (IC) is also calculated using the Bootstrap (BBA) algorithm (Comiso, 1986), and the ASI ice concentration is set to 0% where the Bootstrap ice concentration is below 5% – this is done because the Bootstrap algorithm uses the 18 and 37 GHz channels and is therefore less sensitive to atmospheric phenomena (but has coarser resolution of course). The current version 5.4, along with the previous version 5.3 and 5.2 of the ASI algorithm use the parameter values (tie points and thresholds) given in Table 2.

3.3 Gridding

All swath ice concentration data of one calendar day (with respect to UTC) are resampled (gridded) into various polar stereographic grids using the routine *nearneighbor* of the software package *Generic Mapping Tools* (*GMT*), version 5.2.1. The hemispheric maps (Arctic, Antarctic) use the standard polar stereographic grids of the National Snow and Ice Data Center (NSIDC) at 6.25 km and 3.125 km grid spacing (about the grids, see https://nsidc.org/data/polar-stereo/ps_grids.html). The EPSG code[2] is 3411 for the Arctic and 3412 for the Antarctic grid. An overview of these four regions and the grids is in Table 3
In addition to the four "hemispheric" regions, a number regional maps in 3.125 km grid spacing are being generated as well (but have not been reprocessed in version 5.4). These regional maps use the polar stereographic projection as well but with adapted standard longitudes and latitudes. The standard longitude is the longitude of the meridian that points vertically towards the pole in the projection, the standard latitude is the latitude along which there is no areal distortion, so the grid spacing is the real spacing (areal distortion is between -6% at the poles and +29% at 45° latitude (see also https://nsidc.org/ease/ease-grid-projection-gt)

[2]See http://www.epsg-registry.org/

Region	Grid	grid spacing	parameters	size (pixels)
Arctic	NSIDC North	6.25 km	std lat:70°N,std lon: 45°W	1216 × 1792
Arctic3125	NSIDC North	3.125 km	std lat:70°N,std lon: 45°W	2432 × 3584
Antarctic	NSIDC South	6.25 km	std lat:70°S,std lon: 0°	1264 × 1328
Antarctic3125	NSIDC South	3.125 km	std lat:70°S,std lon: 0°	2528 × 2656

Table 3: *Hemispheric regions and their polar stereographic map projection properties. Note; "std lat" is standard latitude of the projection, "std lon" its standard longitude; "size (pixels)" is x-coordinate (number of columns) by y-coordinate (number of rows).*

3.4 Land masking and coast lines

The land mask and the coast lines for the maps actually come from several sources:

- Land-sea distinction inherent in AMSR-E and AMSR2 swath data: footprints with a non-zero land fraction are excluded.
- Additionally when processing: applying land masks based on GMT5
- During gridding: GMT5 coast lines
- inland lakes (according to GMT5) are excluded.

3.4.1 "Land contamination'

Note that even footprints off the coast can still be influenced by nearby land: The microwave emission of land is in general much higher than the emission from water, and the antenna sidelobes can make the emission from land "contaminate" the signal from the sea received by the antenna main lobe. This can cause erroneous non-zero ice concentration along any coast in a margin of about 20 km for the 89 GHz channel.

3.5 Maximum ice extent masking

To exclude spurious sea ice concentrations over open water in temperate and subtropical regions, caused by atmospheric phenomena like heavy precipitation, a mask of the maximum ice extent during that month in the past 40 years is applied, i.e., ice concentration outside the area of maximum ice extent is set to zero.

4 Validation and Error Characterisation

The ASI algorithm has been validated by comparison with in-situ ice observations and comparison with ice concentration retrievals using other microwave algorithms, and by comparison with ice concentration derived from higher resolution optical sensors (Spreen et al., 2008; Wiebe et al., 2009; Heygster et al., 2009).
The error was estimated based using error propagation from the radiometric error of the brightness temperatures and from the variability of the tie points and of the atmospheric opacity. The absolute error at 0% IC is 25% and decreases for higher IC: at 100% IC it is 5.7%. For high ice concentration above 65%, the error is less than 10% IC (Spreen et al., 2008). For comparison of the ASI algorithm with other sea ice concentration retrieval algorithm see also Ivanova et al. (2015).

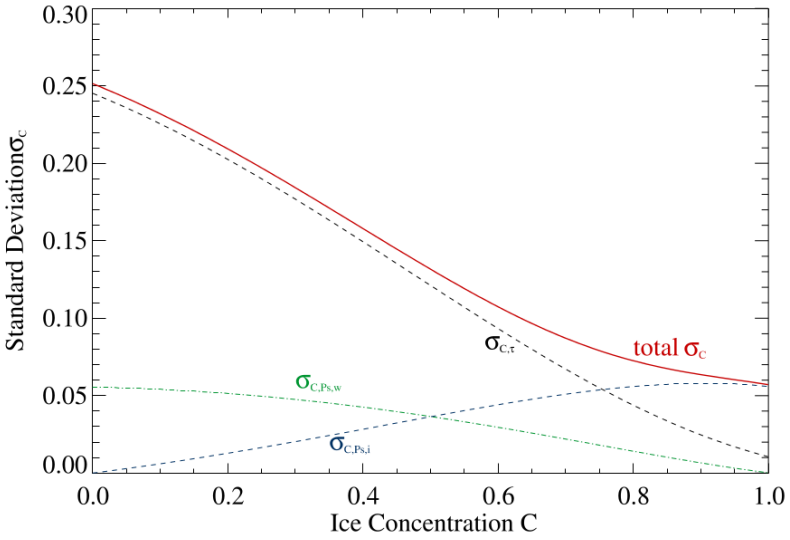

Figure 1: *The expected standard deviation σ_C of the ASI ice concentration C using fixed tie-points as well as the variabilities of the tie points and the atmospheric opacity (from field measurements). Red: total expected standard deviation of C; black dashed: error contribution of atmosphere; green dash-dotted and blue dashed: contribution from variability of open water and sea ice tie point, respectively. Adapted from Figure 9 of (Spreen et al., 2008)*

5 Product Description

The product comes in various formats (detail below):

- HDF4 file containing the gridded ice concentration data
- NetCDF file containing the gridded ice concentration data
- geoTIFF file containing the gridded ice concentration data
- image files (PNG) showing a map of sea ice concentration

Data access is via HTTP or FTP, see https://seaice.uni-bremen.de. The archive directory structure and file naming is best explained by an example:
`data/amsr2/asi_daygrid_swath/n6250/2015/may/asi-AMSR2-20150501-v5.4_nic.png`

where

amsr2 : Sensor; `amsr2` or `amsre`

n : Hemisphere; `n` (North) ors (South)

6250 : Grid resolution in meters; `6250` or`3125`

2015 : Year

may : Month

asi-AMSR2 : Algorithm and sensor; for AMSR-E, it is just `asi`

n6250 : Hemisphere and grid resolution again

20150501 : Year, month and day in the format `YYYYMMDD`

v5.4 : ASI algorithm version: `5.4` for the 2018 reprocessed data, just `5` for previous processing (see below)

nic : Colour scale used in PNG maps for sea ice concentration (see below); `nic` or `visual`

Note that the data in NetCDF format are in separate branches of the directory structure, with yearly directories, Arctic data at
`data/amsr2/asi_daygrid_swath/n6250/netcdf/`
and Antarctic data at
`data/amsr2/asi_daygrid_swath/s6250/netcdf/`

5.1 HDF4

The product comes as HDF4 file containing just one field (2-dimensional): the sea ice concentration (IC) in per cent. The latitude and longitude of each grid cell is stored in static HDF files containing two fields of identical dimensions as the IC field which contain the latitude and longitude; they are found here: https://seaice.uni-bremen.de/data/grid_coordinates/

5.2 NetCDF

The NetCDF files are generated using GDAL and contain the 2-dimensional field of sea ice concentration at6.25 km grid spacing. They also contain the needed projection and grid information and are GIS compatible.

5.3 GeoTIFF

The geoTIFF files are generated using GDAL, using geoTIFF flags compatible with ArcGIS.

5.4 Maps

The maps are produced adding coast lines, land and geographic grid lines to the ice concentration data. Two different colour scales are used: The colour scale by the National Ice Center (NIC), and an intuitive colour scale using only white, grey shades, black and blue. Example maps of one day with both colour scales are shown in Figure 2. In maps with the "visual" colour scale, a static land topography is added while with the "nic" colour scale, land is coloured green or white (Antarctica). Note that the maps are not meant for quantitative data analysis.

A Previous ASI versions

Before the complete reprocessing in autumn 2018, ASI data had the following versions:

5.3 : same as 5.4, but processed day by day in near real time, starting from 2 May, 2017.

5.2 : same tie points and weather filtering as 5.3, but: lakes included, and using GMT Versions 3 and 4 with older coastlines; before 2 May, 2017.

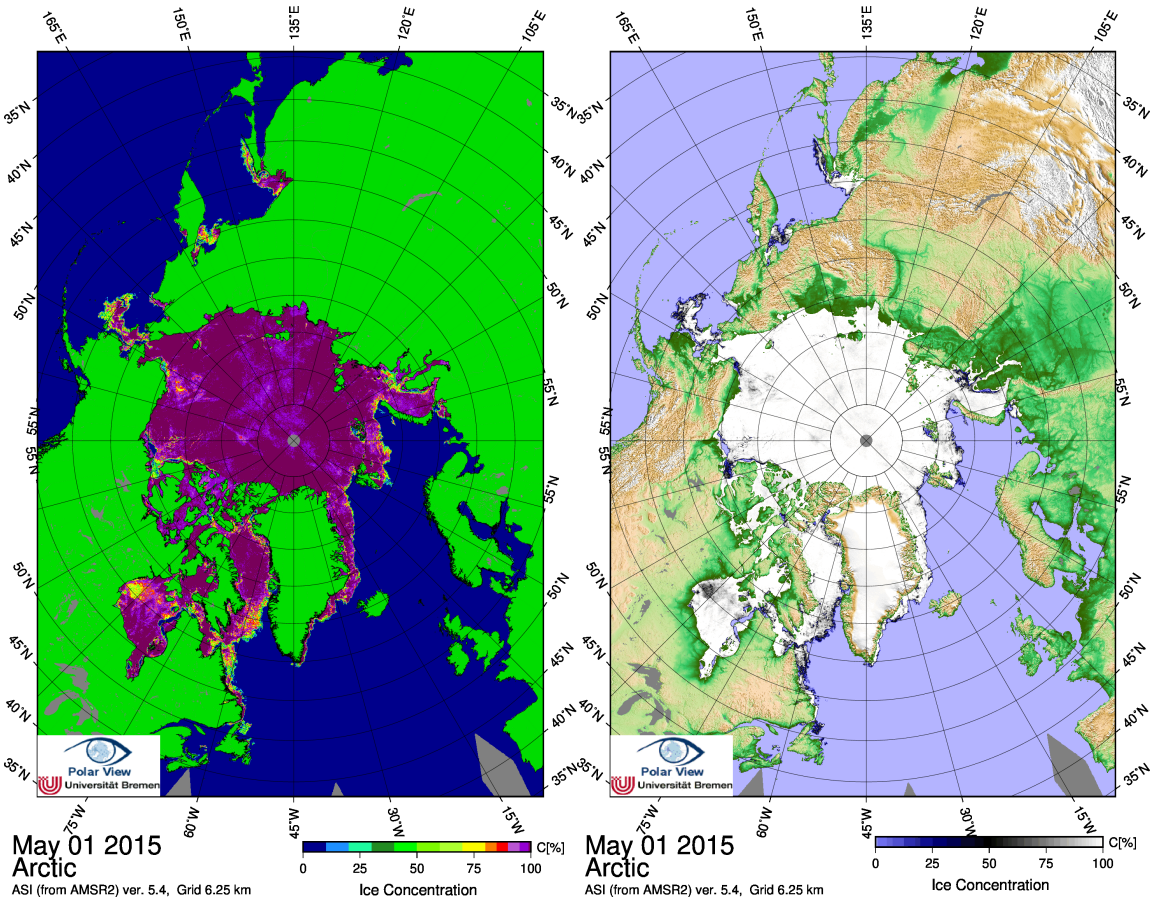

Figure 2: *ASI sea ice concentration in the Arctic on 30 May, 2015, shown in* NIC *colour scale (left) and the* visual *colour scale (right).*

B Coefficients for conversion of AMSR2 T_Bs to AMSR-E T_Bs

The intercalibration coefficients between AMSR2 and AMSR-E brightness temperatures were derived by a linear regression of the differences between AMSR-E and AMSR2 brightness temperatures, ascending and descending swaths combined,

$$T_{B,\mathrm{AMSR2}} - T_{B,\mathrm{AMSR-E}} = s\,T_{B,AMSR2} + i \tag{3}$$

The resulting slope s and intercept i, taken from JAXA (2015) and, for the 89 GHz A scan channels and the 7 GHz channel, from Okuyama and Imaoka (2015), are listed in Table 4. So in order to convert AMSR2 brightness temperatures to AMSR-E brightness temperatures, we have to apply

$$T_{B,\mathrm{AMSR-E}} = (1-s)T_{B,\mathrm{AMSR2}} - i \tag{4}$$

References

J. Comiso. Characteristics of arctic winter sea ice from satellite multispectral microwave observations. *Journal of Geophysical Research*, 91(C1):975–994, 1986.

Channel	Slope s	Intercept i
6V	-0.01390	3.67421
6H	-0.00940	3.03663
7V	-0.00567	2.66603
7H	-0.00702	3.13950
10V	-0.01289	6.34775
10H	-0.00221	3.79624
18V	-0.04524	12.57562
18H	-0.00858	1.89574
23V	-0.00957	4.40435
23H	-0.00947	4.18710
36V	-0.01019	5.49799
36H	-0.00985	4.19181
89V, A scan	-0.01488	5.65119
89H, A scan	-0.04014	12.36275
89V, B scan	-0.01403	5.32379
89H, B scan	-0.00980	3.75174

Table 4: *Coefficient for linear conversion of AMSR2 to AMSR-2 brightness temperatures, from the second intercalibration (JAXA (2015)). Values for the 7* GHz *channels and for the 89* GHz *A-scan channels were taken from the first intercalibration (Okuyama and Imaoka, 2015).*

G. Heygster, H. Wiebe, G. Spreen, and L. Kaleschke. AMSR-E geolocation and validation of sea ice concentrations based on 89 GHz data. *J. Remote Sens. Soc. Japan*, 29(1):226–235, 2009.

N. Ivanova, L. T. Pedersen, R. T. Tonboe, S. Kern, G. Heygster, T. Lavergne, A. Sörensen, R. Saldo, G. Dybkjær, L. Brucker, and M. Shokr. Inter-comparison and evaluation of sea ice algorithms: towards further identification of challenges and optimal approach using passive microwave observations. *The Cryosphere*, 9:1797–1817, 2015. doi: 10.5194/tc-9-1797-2015. URL https://www.the-cryosphere.net/9/1797/2015/.

Japan Aerospace Exploration Agency (JAXA). AMSR-E/Aqua L1A Raw Observation Counts, Version 3. NASA National Snow and Ice Data Center Distributed Active Archive Center, Boulder, Colorado. https://doi.org/10.5067/AMSR-E/AMSREL1A.003, 2003, updated daily. Accessed: September 2018.

Japan Aerospace Exploration Agency (JAXA). Intercomparison results between AMSR2 and TMI/AMSR -E/GMI (AMSR2 Version 2.0). JAXA, https://suzaku.eorc.jaxa.jp/GCOM_W/materials/product/150326_AMSR2_XcalResults.pdf, March 2015. Accessed: October 2018.

T. Okuyama and K. Imaoka. Intercalibration of Advanced Microwave Scanning Radiometer-2 (AMSR2) brightness temperature. *IEEE Transactions on Geoscience Remote Sensing*, 55(8): 4568 – 4577, August 2015. doi: 10.1109/TGRS.2015.2402204.

G. Spreen, L. Kaleschke, and G. Heygster. Operational sea ice remote sensing with AMSR-E 89 GHz channels. In *Proceed. International Geoscience and RemoteSensing Symposium (IGARSS), Seoul, Korea*, page NNN, Piscataway, NJ, 2005. IEEE.

G. Spreen, L. Kaleschke, and G. Heygster. Sea ice remote sensing using AMSR-E 89 GHz channels. *Journal of Geophysical Research*, 113:C02S03, 2008. doi: 10.1029/2005JC003384.

H. Wiebe, G. Heygster, and L. Meyer-Lerbs. Geolocation of AMSR-E data. *IEEE Transactions on Geoscience Remote Sensing*, 46(10):3098–3103, 2008. doi: 10.1109/TGRS.2008.919272.

H. Wiebe, G. Heygster, and T. Markus. Comparison of the ASI ice concentration algorithm with Landsat-7 ETM+ and SAR imagery. *IEEE Transactions on Geoscience Remote Sensing*, 47(9): 3008–3015, 2009. doi: 10.1109/TGRS.2008.919272.